Energy 78 (2014) 373–383

Contents lists available at ScienceDirect

Energy

journal homepage: www.elsevier.com/locate/energy

In-situ and *ex-situ* measurements of thermal conductivity of supercapacitors

H.H. Hauge [a], V. Presser [b, c], O. Burheim [d, *]

[a] Dep.of Chemistry, NTNU–Norwegian University of Science and Technology, 7491 Trondheim, Norway
[b] INM–Leibniz Institute for New Materials, 66123 Saarbrücken, Germany
[c] Saarland University, 66123 Saarbrücken, Germany
[d] Dep. of Electrical and Computer Engin., HiST–Sør-Trøndelag University College, 7004 Trondheim, Norway

ARTICLE INFO

Article history:
Received 9 June 2014
Received in revised form
29 September 2014
Accepted 6 October 2014
Available online 11 November 2014

Keywords:
Thermal conductivity
Supercapcitors
Measured temperature profiles
Thermal behaviour

ABSTRACT

Thermal signature of supercapacitors are investigated *in-situ* and *ex-situ* using commercial supercapacitors.

Regarding the *in-situ* method, four supercapacitors were connected in series, with thermocouples embedded between the supercapacitors. As the applied current was increased, the temperature measured at the intrinsic positions also increased. When cycling at a current density of 0.11 A cm^{-2} the centre temperature increased by 14 K compared to the stack surface temperature. This is an important figure as literature states that an increase of 10 K leads to a corresponding decrease in the lifetime by a factor of 2. Using the obtained temperature profiles, the effective thermal conductivity of the stack was found to vary between 0.5 W K^{-1} m^{-1} and 1.0 W K^{-1} m^{-1}, depending on the compaction of the stack.

For the *ex-situ* measurements, the thermal conductivity and the thicknesses of the supercapacitor material layers were measured individually in order to determine the corresponding thermal conductivity of the stack. When using this method an effective thermal conductivity of the stack of 0.53 ± 0.06 W K^{-1} m^{-1} was obtained. The analysis also demonstrated that the main contributor to the thermal resistivity and conductivity of the supercapacitor construction is the electrodes. This demonstrates that when managing heat from supercapacitors it is important to focus on the thermal conductivity of the components materials.

1. Introduction

Energy management is a key factor for a prosperous human society. Supercapacitors, also known as electric double-layer capacitors or ultracapacitors [1], play a vital role in the technological evolution as their key attributes of high power density makes them preferred over batteries in a wide range of applications [2–4]. Today supercapacitors are found in devices ranging from regenerative breaking systems in electric cars, aiding data storing in computers, as well as to accelerate wind turbines after a period with little wind, or to prevent electrical drop-outs in solar panels [5–8]. Moreover, combined DC (direct current) energy storage hybrids can supply better power quality and demand less space when containing supercapacitors [9] and micro grids with fuzzy powers can be stabilised [10,11].

A major advantage of supercapacitors is their high power density per mass compared to, *e.g.* batteries. A simple way to compare energy storage and power source devices is to compare them in a so-called Ragone plot; a log–log diagram with the energy density (in k Wh kg^{-1}) plotted as a function of the power density (in W kg^{-1}) [12,13]. The reason for the different performances of batteries and supercapacitors in the Ragone plot, lays in the nature of how they store the electric energy [14]. In batteries the energy is stored by using electrochemical reactions, whereas supercapacitors store energy purely by electrosorption of ions on the surface of the carbon electrodes [15]. This allows supercapacitors to obtain a high power density at the cost of a moderate energy density, whereas batteries display the opposite trend [16]. This fact implies that supercapacitors are well suited for applications where energy uptake and supply has to happen fast, *i.e.* power management, whereas batteries are better suited for long-term energy supply, *i.e.* energy management.

The emergence of supercapacitors is closely related to the development of carbon electrode materials, electrolytes, and the

* Corresponding author.
E-mail address: odneb@hist.no (O. Burheim).

http://dx.doi.org/10.1016/j.energy.2014.10.022

design of the supercapacitor units and systems [1]. Today commercial supercapacitors are based on organic electrolytes [17] and film electrodes made from a blend of porous carbon (usually activated carbon; 85–95 wt%), polymer binder (5–10 wt%), and additives to improve the electrical conductivity [18,19]. Several reviews on the electrode materials and electrolytes used in supercapacitors have been published over the last years [2,18,20–22], supplemented with best practice papers with guidelines for testing [23–25], studies on the degradation and ageing of supercapacitors [26,27], and perspectives on current trends and future potentials of this technology [3,19,28].

The *thermal* conductivity of supercapacitors has not been studied in such detail as the respective *electrical* conductivity. Some studies dealing with system cooling and thermal effects have been published [17,29–34], but only few deal with thermal gradients and thermal conductivity directly [31,33] applying values that are not obtained specifically for supercapacitor components. For the activated carbon component film electrodes, the dry thermal conductivity of graphite [35], graphene [36], and carbon nanotubes [37], among other carbon materials has been reported in the range of 0.1–0.2 W m^{-1} K^{-1}. This is the same range of values reported for activated carbon measured in air [38]. To our knowledge, only one study reports the thermal conductivity of various types of supercapacitor electrodes both dry and soaked in electrolytes [39].

In the light of scarce literature on the internal temperature handling of supercapacitors the aim of this study is to supply data on electrode heat management, and also to elucidate heat bottlenecks in design of supercapacitor systems. The paper will aid this process by studying the *thermal* conductivity, and temperature profiles, of commercial supercapacitor materials through *in-situ* and *ex-situ* methods.

2. Theory

In order to determine the thermal conductivity of the supercapacitors, λ, an *in-situ*, and an *ex-situ* experimental approach is applied in accordance with theory on transport phenomena described by Bird et al. [40]. The *in-situ* method, method I, seeks to determine the overall thermal conductivity of a stack of four supercapacitors connected in series using a sum of least squares method to fit the thermal conductivity to the internal temperature gradient, the ohmic resistance, and the geometry of the stack. The *ex-situ* method, method II, uses an apparatus and an experimental method developed by Burheim et al. [39,41–43] in order to determine the individual through-plane thermal conductivities of porous carbon particle based materials such like those in supercapacitor electrodes. The *ex-situ* method will serve as a reference for the *in-situ* method, as the thermal conductivity of the supercapacitor constituting materials can be 'summed up' to the overall conductivity of the capacitors. Combining these two techniques in a single study creates a unique framework for studying and evaluating the thermal conductivity from a sub-component level and up to a large scale level of several supercapacitor units.

2.1. Method I: in-situ measurements

This section is dedicated to define the thermal conductivity, λ, from a stack of supercapacitors used in an isothermal calorimetric study. The experimental equipment used for this method is displayed in Fig. 3, which will be more thoroughly described in the experimental section. The flux of internal energy from the stack of supercapacitors, $\dot{U}$, is defined according to the first law of thermodynamics, in Eq. (1):

$$\dot{U} = \nabla(\lambda \nabla T) + \dot{Q} = 0 \tag{1}$$

where λ is the thermal conductivity, $\dot{Q}$, is the volumetric ohmic heat generation, and ∇ is the cartesian vector differential operator. When a system is thermally insulated in the y- and z-directions, as in our experimental set-up, the heat fluxes can be considered to be a one-dimensional one and one is left only with gradients in the x direction, *i.e.*;

$$\lambda \frac{\partial^2 T}{\partial x^2} = -\dot{Q} \tag{2}$$

The volumetric heat of the supercapacitors can be averaged to Eq (3):

$$\dot{Q} = \frac{Q_{\text{total}}}{V} = \frac{RI^2}{wh\delta} \tag{3}$$

where Q_{total} is the total heat generated by the supercapacitors, V is the volume of the supercapacitor stack, R is the electrical resistivity of the stack, I is the current entering the stack from the cycling unit, and w, h, and δ represent the width, the height, and the thickness of the supercapacitor stack, respectively.

Fig. 1 shows a sketch of the four supercapacitors as they are used in the experiments. In Fig. 1 the numbering of the various temperature measurements are indicated, from T_1 through T_5, with the maximum temperature measured at T_3. Of temperature profiles, displayed in the results, measurement spots are distributed symmetrically about the maximum temperature in the middle of the stack, T_3's geometrical position is used as the origin of the model: $x(T_3) = 0$. The total thickness of the stack of supercapacitors is represented by the greek letter δ. As illustrated in Fig. 1, the measurement points of the temperatures T_1 through T_5, are set at equal

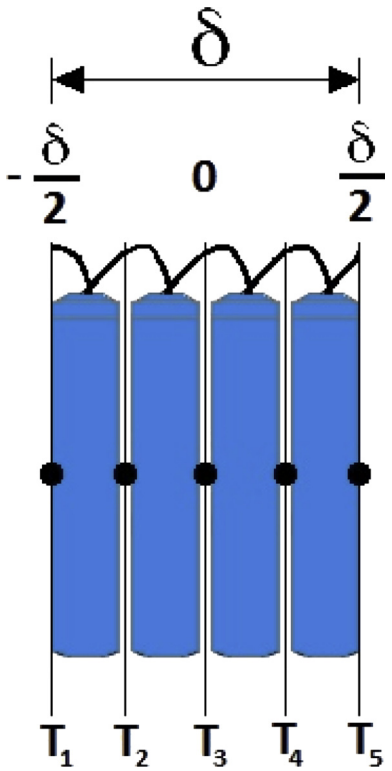

Fig. 1. Cross section of the capacitor stack with the placement of the thermocouples indicated.

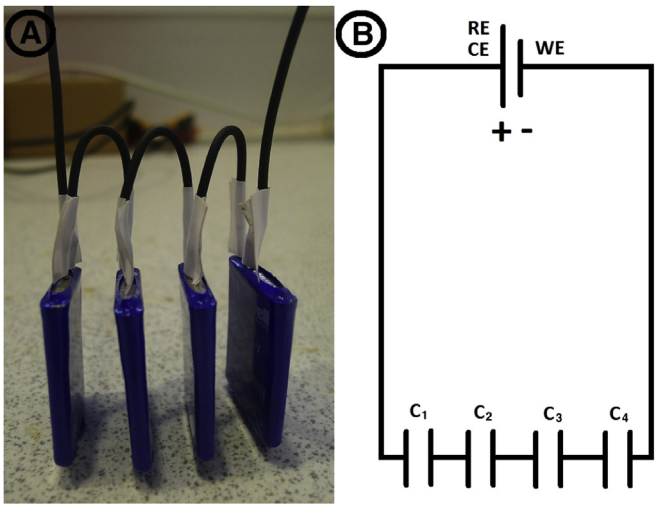

Fig. 2. Image of the Maxwell PC10 supercapacitor stacks with four supercapacitors coupled in series (A), and the corresponding electric circuit (B). The circuit connection to the PAR 263A leads, (WE), (CE), and (RE), are indicated.

distances of $\delta/4$ apart from each other, ranging from $x(T_1) = -\delta/2$, to $x(T_5) = \delta/2$, relative to origin.

Defining $x = 0$ in the middle of the stack, the boundary conditions for the system becomes Eqs. (4) and (5).

$$T = T_0, \quad \text{when } x = \pm\frac{\delta}{2} \tag{4}$$

where T_0 is the reference temperatures measured by the thermocouples at the axial boundaries of the stack, at T_1 and T_5.

$$\frac{\partial T}{\partial x} = 0,4 \quad \text{when } x = 0 \tag{5}$$

Solving Eq. (3) using the boundary conditions given in (4) and (5) under the assumption that the ohmic heat is uniformly distributed and that the effective thermal conductivity, λ_{eff}, is isotropic and uniform, we obtain Eq. (6). Eventually, we are interested in the temperature difference throughout the stack, $\Delta T(x)$, and to fit this to the measured temperature differences, $\Delta T_{i-j}(x)$, where $i - j$ represent the five thermocouples in Fig. 1 and Eq. (7) becomes a more convenient expression.

$$T(x) - T_0 = \frac{RI^2}{2\lambda_{\text{eff}} wh\delta}\left(\frac{\delta^2}{4} - x^2\right) \tag{6}$$

$$\Delta T(x) = \frac{RI^2}{2\lambda_{\text{eff}} wh\delta}\left(\frac{\delta^2}{4} - x^2\right) \tag{7}$$

By fitting the points of the temperature measurements from the experimental data to the expected temperature difference in Eq. (7), the effective thermal conductivity, λ_{eff}, can be determined by using a least sum of least squares approach. The sum of least squares, SoLS, of the difference between the experimental and modelled temperature difference, is found by fitting the effective thermal conductivity to the known parameters. This is done by minimizing the difference between the measured temperature difference and the modelled parameters, with respect to the effective thermal conductivity, λ_{eff}, which is assumed to be constant through the stack, as expressed in Eq. (8).

$$\text{SoLS} = \frac{\partial \Sigma(\Delta T_i - \Delta T(x))^2}{\partial \lambda} = 0 \tag{8}$$

where ΔT_i indicate the difference between the experimental temperature measurements, at T_1 through T_5, relative to the reference temperature (equal to the average between temperature T_1 and T_5), and $\Delta T(x)$ is the corresponding modelled temperature difference relative to the reference temperature and Eq. (7). The modelled thermal conductivity with a minimum in the SoLS is defined to be equal to the experimental effective thermal conductivity, λ_{eff}.

2.2. Method II: ex-situ measurements

The theory of this experimental method is based on a well established method which has been used to determine the thermal through-plane conductivity of similar materials earlier [39,41–43]. The apparatus used for the experimental procedure is described in the experimental section and illustrated in Fig. 4.

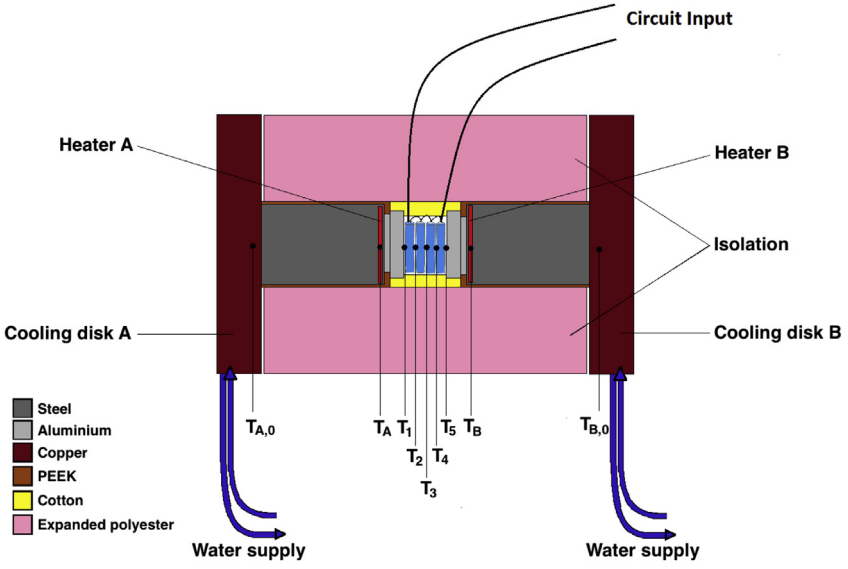

Fig. 3. Experimental set-up of the supercapacitor stack sandwiched in the calorimeter, as described in the text.

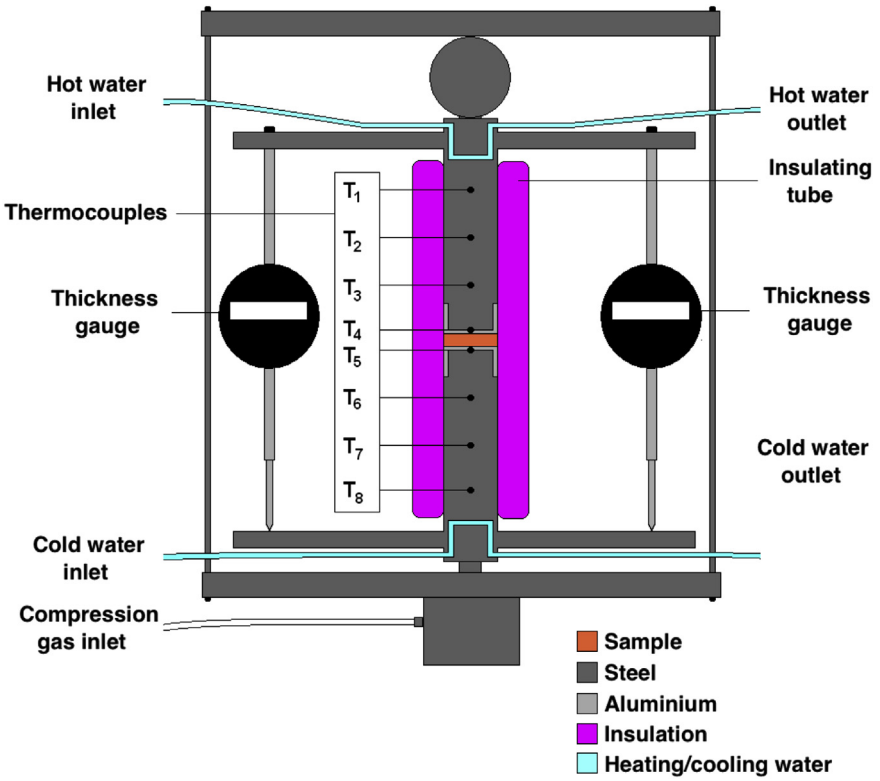

Fig. 4. Apparatus for experiments on sample thermal through-plane conductivity, λ.

This method uses an induced known heat flux that is led through the steel cylinders of the apparatus, sandwiching the sample, to determine the thermal conductivity. The apparatus provides a vertical 1D heat flux from the top to the bottom of the apparatus through the steel cylinders and the sample, both with a diameter of 21.0 ± 0.1 mm. Temperatures are measured at three positions in each of the steel cylinders at T_1–T_3 and T_6–T_8, in the upper and the lower cylinder, respectively, in order to ensure and determine the presence of the 1D heat flux, as illustrated in Fig. 4. Additionally, the temperatures at each side of the sample (T_4 and T_5) are measured in order to determine the temperature drop across the sample. As described in the experimental section, the apparatus can be used to measure the sample thickness at a certain compaction pressure which makes it possible to recreate the expected compaction pressure within supercapacitors. The thicknesses of the samples are varied by stacking sample layers on top of each other inside the apparatus.

Each of the two cylinders are operating as a kind of heat flux meter. The heat flux through the steel is obtained from the known thermal conductivity of the steel used in the construction, together with the change in temperature between the outermost temperature measurements, T_1 and T_3, and T_6 and T_8, as displayed in Eqs. (9) and (10), for the upper and lower cylinder, respectively.

$$\dot{q}_{\text{upper}} = \frac{\lambda_{\text{steel}}(T_1 - T_3)}{\delta_{1-3}} \tag{9}$$

$$\dot{q}_{\text{lower}} = \frac{\lambda_{\text{steel}}(T_6 - T_8)}{\delta_{6-8}} \tag{10}$$

The heat flux through the sample is set equal to the average of the two heat fluxes, $\dot{q}_{\text{lower}}$ and $\dot{q}_{\text{upper}}$, as shown in Eq. (11).

$$\dot{q}_{\text{sample}} = \frac{\dot{q}_{\text{upper}} + \dot{q}_{\text{lower}}}{2} \tag{11}$$

Having determined the heat flux through the sample, the area specific thermal resistance, r, can be calculated from the temperature drop from T_4 to T_5 divided by the heat flux, from Eq. (12).

$$r_{\text{sample}} = \frac{T_4 - T_5}{\dot{q}_{\text{sample}}} \tag{12}$$

The thermal conductivity is obtained using the geometric proportions of the sample, namely the thickness at a given compaction pressure, δ_{sample}, the area, A_{sample}, and the area specific thermal resistance of the sample, r_{sample}. This is shown in Eq. (13).

$$\lambda_{\text{sample}} = \frac{\delta_{\text{sample}}}{r_{\text{sample}} A_{\text{sample}}} \tag{13}$$

This method will be used to obtain the thermal conductivities, and resistivities of all the materials constituting the supercapacitor, λ_i and r_i. When all the sample thermal conductivities are obtained, the total resistance of the supercapacitor stack can be calculated from the total thickness of each constituent in the supercapacitor stack using Eq. (14).

$$r = \sum_i r_i = \sum_i \frac{\delta_i}{\lambda_i A_i} \tag{14}$$

To obtain the overall thermal conductivity, λ, the total thickness of the supercapacitor stack, δ, the axial area (corresponding to the area facing the aluminium plate in the calorimeter), A, and the total thermal resistance, r, are inserted in Eq. (15).

$$\lambda = \frac{\delta}{rA} \tag{15}$$

The value for the thermal conductivity from Eq. (15) will be compared to the value with the smallest sum of least squares in Eq. (8) and from that the validity of the two models will be determined.

3. Experimental

Maxwell PC10 Series supercapacitors have been selected for investigation. In these experiments four supercapacitors are connected in series with wires, as shown in Fig. 2. In this way they are expected to behave as one single supercapacitor, while giving access to the internal temperature gradients of the stack. In order to determine both the effective thermal conductivity of the supercapacitor units and of their subcomponents a calorimeter [44] and an apparatus specifically designed for thermal conductivity measurements [39] of dissected material samples were used. In Table 1 relevant data of the supercapacitors from the manufacturer are presented [45].

3.1. Experiment I: in-situ measurements

In order to test the efficiency of the supercapacitor stack during use, the stack was cycled by charging and discharging repeatedly leading to a stationary thermal state. The isocalorimetric experiment was carried out with a boundary temperature of 30 ± 0.1 °C in a calorimeter which will be described in detail later in this section. A PAR 263A (Princeton Applied Research 263A potentiostat/galvanostat) was used to charge and discharge the stack while logging the heat and the temperatures. The PAR 263A was controlled by a computer through a Corrware software operating in a galvanostatic mode which also recorded the cycling data of the applied currents and voltages. The supercapacitor stack was cycled stepwise at currents increasing from 0 A to 2 A, with current intervals of 0.125 A, charging and discharging between voltages of 0 V and 2 V for 100 charge/discharge cycles per current level. In this way we were able to run the supercapacitors galvanostatically at different currents and in a way such that the heat would be stationary. The circuit scheme of the supercapacitor stack is displayed in Fig. 2(B) together with a photo of the supercapacitor stack in Fig. 2(A). In the coupling scheme the four supercapacitors are marked with the conventional capacitor sign, and the letter C. The working, counter, and reference electrodes are indicated by WE, CE, and RE, respectively, indicating the connection to the PAR 263A.

Moreover, several stacks of supercapacitors were assembled as shown in Fig. 2(A). Each of these set-ups are labelled by a letter (A, B, or C). These set-ups were cycled as described above and the results analysed to obtain an effective thermal conductivity, λ_{eff}. The procedure was repeated at least three times in order to ensure reproducibility. The reproductions are later on indicated by numbers, *i.e.*, B1, B2, and B3 for the B set-up.

The calorimeter accommodating the supercapacitor stack is sketched in Fig. 3 The boundary surface temperatures, T_A and T_B, were maintained by the calorimeter, originally designed for measuring the heat leaving the cathode and anode side of a fuel cell [46]. The calorimeter was modified by adding holders at the internal axial surfaces in order to fit the shape of 40 mm × 40 mm thermoelectric generators. An overview of a cross section of the calorimeter experimental set-up is given in Fig. 3.

Table 1
Specifications given by the manufacturer, Maxwell Technologies [45].

Specification	
Capacitance	10 F
Absolute maximum voltage	2.70 V
Applicable temperature range	−40 °C to 70 °C
Lifetime	500,000 cycles[a]

[a] Validity; from rated voltage to half the voltage. Cycling performed at a duty cycle resulting in no heating of the ultracapacitor and with the ultracapacitor maintained at 25 °C.

The calorimeter is constructed as a cylinder with insulation at the radial walls and heat transport in the axial directions. The calorimeter consists of two symmetrical pieces making it possible to distinguish between heat leaving at either side of the supercapacitor stack. This is done by generating a heat flux from the two heaters in the direction to the cooling disks. The calorimeter is built primarily in steel, copper, aluminium, PEEK (poly ether ether ketone), and expanded polyester. The cooling disks are made from copper due to its high thermal conductivity which is well suited for cooling from the water-bath through copper pipes soldered onto the outer copper disks. The cooling liquid is supplied from a Grant R1 low temperature bath/circulator set to a temperature of 10 °C giving temperatures of approximately 10 °C at the cooling disks. High conductivity is also required at the interface adjacent to the device to be tested; therefore, aluminium is the building material of the 40 mm × 40 mm plates facing the supercapacitors. The housing of the two symmetrical parts of the calorimeter is made from PEEK due to its thermal and electric insulation properties and its mechanical strength. The radial insulation between the copper cooling plates are made of expanded polyester and additional cotton was placed around the supercapacitor stack in order to maximize the insulation in the y- and z-directions. In order to maximize the thermal conductivity in the axial direction, thermally conductive paste was greased at all axial interfaces of the supercapacitors and also between all connecting axial interfaces in the calorimeter itself. Four bolts running through the calorimeter in the axial direction were additionally tightening the apparatus in a symmetrical way using an electric hand drill with a fixed torque. The torque was fixed in order to avoid mechanical damage to the supercapacitors.

The heat from the heaters and the temperatures were logged using a LabView interface. The temperatures (at the heaters, the cooling disks, and at interfaces of the supercapacitors) were measured using K-type thermocouples. The positioning is indicated in Fig. 3. The temperature at the heaters and the cooling disks, T_A and T_B, and $T_{A,0}$ and $T_{B,0}$, respectively, were used to control that a temperature gradient was present and stable through the steel cylinders. The heaters were controlled using two Eurotherm thermostatic PID-controllers regulating the effect applied to the resistive heating wires, relative to the temperature measured at T_A and T_B. In order to ensure a certain temperature at the interface between the supercapacitor and the calorimeter, the temperature set point of the heaters was adjusted in order to obtain a temperature of 30 ± 0.1 °C at either side of the supercapacitor stack (T_1 and T_5). The ohmic resistance was measured during an initial calibration before the cycling was initiated. The thermocouples giving the temperatures at the interstitial positions of the supercapacitor stack, T_1–T_5, gives the internal temperature gradient of the supercapacitor stack during cycling.

3.2. Experiment II: ex-situ measurements

In section 2.2 the method for obtaining the thermal conductivity of the supercapacitor materials is presented. Materials obtained from dissections of the supercapacitors were investigated using an apparatus previously used in numerous experiments on thermal through-plane conductivity of nano porous carbon materials [39,41–43] depicted in Fig. 4. The apparatus is designed to generate a constant 1D heat flux through the sample of a cylindrical

geometry. As displayed in the figure the samples are sandwiched between the two symmetrical metal cylinders (both with a 21 mm diameter). The samples were inserted as single layers and then stacked on top of each other (in increasing numbers) in order to vary the sample thickness. The sample thicknesses were measured as a function of the compaction pressure applied vertically from the bottom to the top of the apparatus. The thickness of the sample was measured using two Mitutoyo Digimatic Indicator ID-C Series 543 attached to the upper flange touching down onto the lower flange with the measuring tip as illustrated in Fig. 4. The change in distance, relative to calibrations done without samples inside the apparatus, represents the thickness of the sample at a given compaction pressure.

The mobile parts of the apparatus are confined between two steel plates which are attached to each other with four bolts. The compaction pressure is applied compressed air gas bottle which is connected to a pneumatic piston located below the lower steel plate. The pneumatic piston pushes the internal cylinders upwards against a steel ball held by the upper steel plate, thus compressing the sample between the heat flux pistons. The heat flux is generated by two fluxes of hot and cold water, passing through the top, and bottom end of the internal cylinders, respectively. The cold water flux (mixed with glycolic antifreeze) was obtained from a Grant R2 low temperature bath/circulator and the hot water flux from an in-house made heating bath that circulates water in an external tube. The temperature of the cold and hot water was regulated to 5 °C and 40 °C, respectively, which provided a temperature gradient through the cylinders and the sample. The temperatures fitting the model described in section 2.2 are measured using eight K-type thermocouples indicated with T_1 through T_8 in Fig. 4. All eight temperatures were recorded using an Agilent acquisition switch unit 34970A. Radial insulation is assured with a tubular dewar (double-walled evacuated glass tube coated with silver at the inside walls) and further insulated with a soft polymer insulation material on the outside.

The two symmetrical cylinders are made from steel from the flanges to the interface towards the sample, which is coated with a thin aluminium layer. The relatively intermediate thermal conductivity of steel makes it a well suited material to achieve a thermal gradient and a high resolution of the heat flux. The cap facing the sample is made of aluminium because the high thermal conductivity creates an almost isothermal region adjacent to the sample where the thermocouple is and thus allows one to determine the temperature drop across the sample. Two sets of three thermocouples are placed inside the upper and lower steel cylinders in order to measure the temperature at T_1–T_3 and T_6–T_8, respectively. This is done in order to assure the presence of a linear temperature profile through the steel sections. From these temperature measurements the heat fluxes through the upper and lower cylinders are determined. Thermocouples were also placed at each interface between the steel and aluminium cap, at T_4 and T_5, thus making the cap behave as a thermometer disk yielding the temperature drop across the sample.

The samples of the separators, the carbon/aluminium electrodes, the aluminium current collectors, and the plastic coating were cut into 21 mm disks fitting the surface of the aluminium cap of the steel cylinders. The samples of the separator and the electrodes were also soaked in 1 M tetraethylammonium-tetrafluoroborate (TEA BF_4) dissolved in acetonetrile in order to reproduce the electrolyte inside a supercapacitor in accordance with a recent study [39]. The experiments were done first with a single layer stack and then three more stacks of samples with increasing number of samples in each stack. The thickness and thermal resistivity of the sample stacks were measured with 2.3 bar intervals; first by compressing the samples from 4.6 bar to 16.1 bar and then by decompressing the samples back down to from 4.6 bar. The temperature measurements were carried out every 15 s for 15 min at 4.6 bar, 9.2 bar, 13.6 bar and 16.1 bar during compression and at 4.6 bar during decompression. Only the last 5 min of the temperature measurements were used for determining the thermal conductivity, in order to be sure to have stationary conditions.

4. Results and discussion

In the following the results from the experiments described in the experimental section 3 are presented as average values with 95% confidence intervals.

4.1. Supercapacitor components and geometry

In Fig. 5 the internal assembly of the supercapacitor is displayed. The folded section represents the capacitor section of the supercapacitor unit and is illustrated in more detail in Fig. 6. The main components in the capacitor section are the aluminium current collectors, the paper separator, and the carbon/aluminium electrodes. The vertical lines in the figure illustrate the folds and the numbered arrows indicate the order in which the folding is performed. In Table 2 the thicknesses of the supercapacitor components and the number of layers through the supercapacitor stack in the axial direction are presented. The area of the electrodes was found to be $A_{electrode} = 2.5 \pm 0.1\ cm \times 7.2 \pm 0.1\ cm = 18.0 \pm 0.7\ cm^2$.

4.2. Effective thermal conductivity: the in-situ measurements

In the following the results from the isothermal calorimetry of the supercapacitors are presented. The measurements were carried out at a reference temperature of 30 ± 0.1 °C. Three supercapacitor stacks are presented when cycling the supercapacitor stacks between positive and negative potentials of 2 V and increasing the

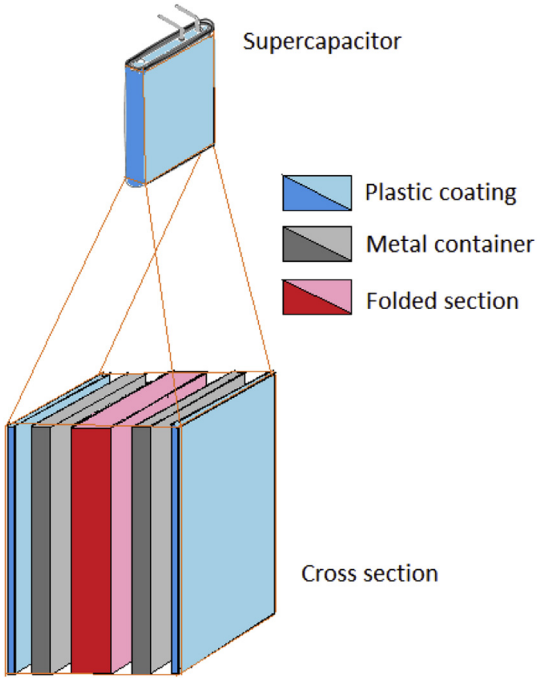

Fig. 5. Internal assembly view a supercapacitor unit: The plastic coating is indicated in blue, the metal container in grey, and the folded capacitor section is indicated in red/pink in the middle of the cross section. (For interpretation of the references to colour in this figure legend, the reader is referred to the web version of this article.)

applied current stepwise with intervals of 0.125 A from no applied current (during calibration) to a maximum current of 2.0 A. As seen from the graphs in Fig. 7, where a current of 1.0 A is applied while alternating the voltage between −2 V and 2 V. In practice, cycling the supercapacitors between positive and negative potentials means changing the charge of the electrodes, forcing the ions of the electrolyte to travel back and forth between the electrodes. Yet, commercial supercapacitors are typically charged and discharged while keeping the positive electrode positive and the negative. In this study, however, we are primarily interested in the ohmic effect of the charging/discharging processes and, therefore, swept the current for longer before alternating it.

4.2.1. Temperature profiles

The temperature profiles obtained during the cycling of the supercapacitors showed a clear second order polynomial trend. This is in agreement with the theory of method I (Eqs. (6) and (7)). From Fig. 8 it is evident that the temperature increases in response to the increase in applied current. 7 experimental set-ups were investigated in total and the three latest are presented here under the labels A, B, and C. For each set-up several repetitions were carried out. The temperature profiles obtained in the experimental series for a single supercapacitors stack (in experiment A1 to A3, B1 to B3, and C1 to C3) show almost no deviations within each reproduction series. No mechanical adjustments were carried out between each experiment in an experimental series which is most likely the reason why the temperature profiles are as highly reproducible as exemplified in Fig. 9. The temperature profiles of the A and C series experiments showed similar reproducibility. When changing the supercapacitor stack, sandwiched in the calorimeter, the temperature profiles are lower for the B and C series than for the A series and the C series temperature profiles are lower than temperature profiles of the B series. The temperature profiles of experiment A1, B1 and C1 are presented in Fig. 8. A possible reasons for the change in the temperature profiles of the A, B, and C set-ups is either a decrease compression of the stack inside the calorimeter or the fact that the ohmic resistance of the supercapacitor stacks in the B and C series experiments are lower than the ohmic resistance of the stack used in the A series experiments. The slight decrease in the ohmic resistance (Table 5) of the B and C series supercapacitor stacks, compared to the A series stack, does not explain the decrease in temperature profiles between the respective stacks. Therefore, the compaction pressure is assumed to be the most important factor for the temperature dependency.

The temperature at the interface between the supercapacitor stack and the aluminium plates of the calorimeter is set to 30 ± 0.1 °C during the calibration at zero current. As the applied current is increased, the temperature at the respective interface has typically increased to approximately 0.4 to 0.6 °C higher than the initial temperature when reaching 2.0 A. This is due to a contact between the aluminium and copper with the heaters). The increase in temperature at the interface is adjusted for in the approximation of the thermal conductivity in method I.

The symmetry of the temperature profile is an important observation when calculating the thermal conductivity, using method I, as it is crucial for the validation of the method. The second order symmetry of the temperature profiles become even more evident when the maximum temperature measured at thermocouple position T_3 is plotted as a function of the applied current squared, I^2, as presented in Fig. 10. In this plot it is clear that a significant change in temperature takes place when the cycling current exceeds 1.375 A. This is also observed when modelling the thermal conductivity, using method I. We explain this in the following sections.

Table 2
Supercapacitor layer characteristics for a stack of four Maxwell PC10 supercapacitors.

Material	Number of axial layers	Layer thickness [mm]	Total thickness [mm]
Plastic coating	8	0.108 ± 0.026	0.862 ± 0.205
Steel housing	8	0.331 ± 0.111	2.648 ± 0.886
Big aluminium current collectors	16	0.057 ± 0.013	0.910 ± 0.213
Small aluminium current collectors	4	0.041 ± 0.006	0.165 ± 0.025
Separator	16	0.066 ± 0.015	1.052 ± 0.233
Carbon/alumininum electrodes	32	0.223 ± 0.008	7.120 ± 0.258
Electrode aluminium layer	32	0.040 ± 0.016	1.280 ± 0.504
Electrode activated carbon layer	32	0.183 ± 0.018	5.840 ± 0.563

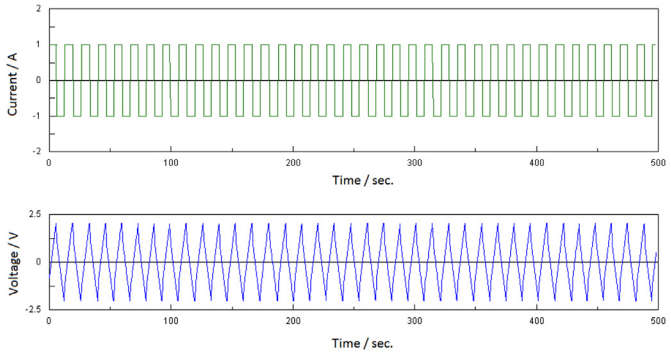

Fig. 7. Example of the applied currents and voltages during the first 500 s of cycling of the supercapacitor stack. Here for cycling between positive and negative voltages of 2.0 V, and corresponding positive and negative currents of 1.0 A (corresponding to a current density of approximately $j = 56$ mA cm^{-2}).

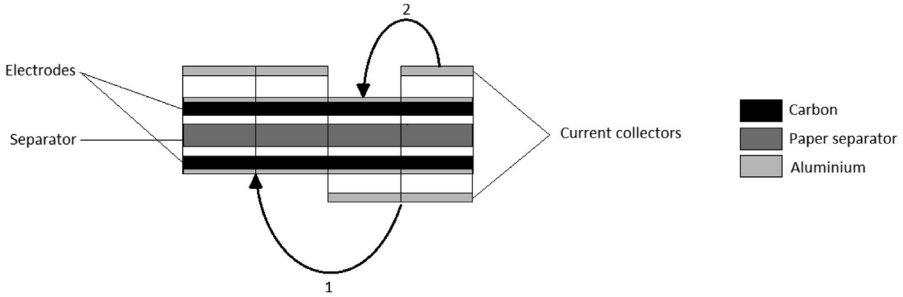

Fig. 6. Illustration of the unfolded capacitor section, consisting of aluminium current collectors, a separator, and carbon/aluminium electrodes. The vertical lines illustrates where the folds originally are and the numbered arrows indicate the order of the folding.

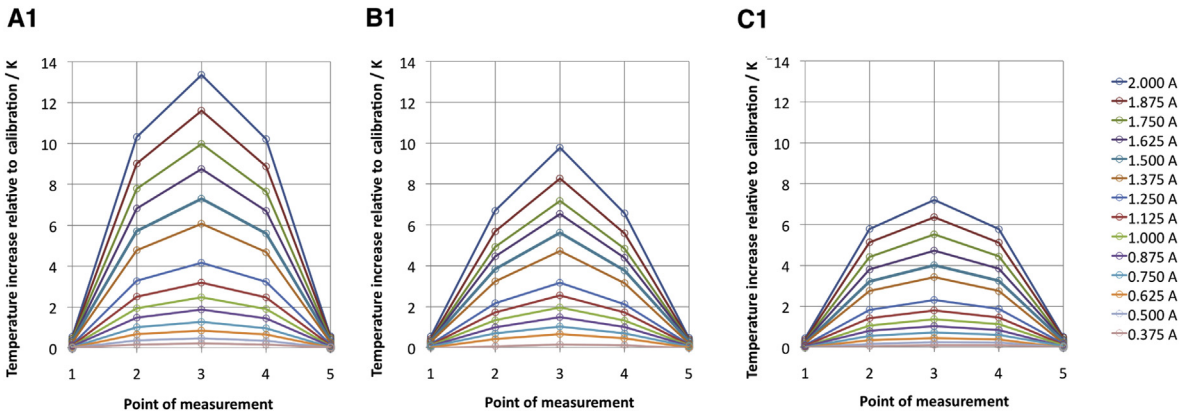

Fig. 8. Temperature profiles of experiment A1, B1 and C1.

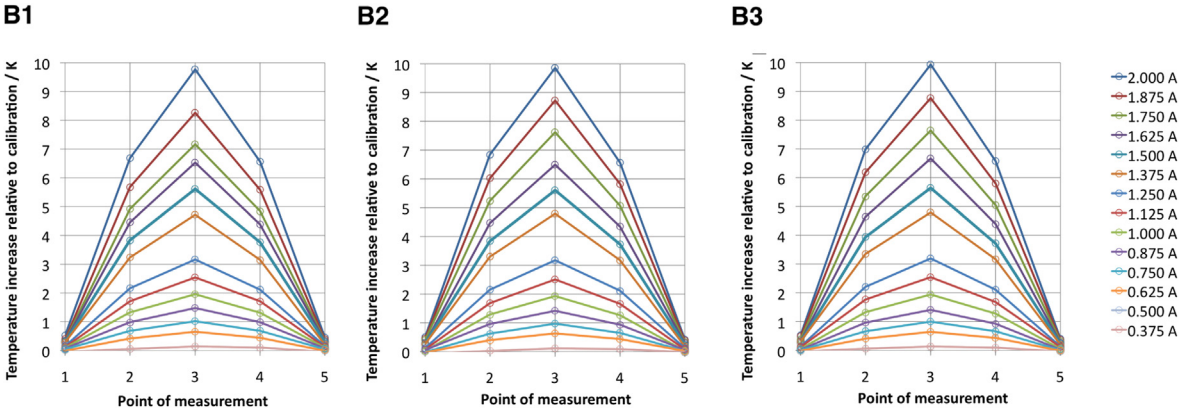

Fig. 9. Temperature profiles from the three different series (B1-3) with set-up B.

4.2.2. Thermal conductivity

In Fig. 11 the thermal conductivities of the supercapacitor stack, λ_{stack}, obtained by using the sum of least squares method are plotted as a function of the applied current for experiment A1, B1, and C1. In Table 3 all the thermal conductivities from the three experimental series are presented. As the increase in temperature is higher in the A series experiments compared to the B and C series experiments, the respective thermal conductivities, λ_{stack}, in these experiments are also higher as the temperature increase is expected to arise from the thermal resistivity of the supercapacitor materials which evidently is lower in the B and C series experiments than in the A series experiments.

The temperature profiles of the three experiments within each experimental series are approximately equal as illustrated earlier; therefore, their respective thermal conductivities are also fairly similar as can be seen from Table 3. The fact that the thermal conductivities reaches a steady value at 1.375 A and higher indicates that the heat production can be regarded as insignificant for determining the thermal conductivity at the lower current densities.

By rearranging Eq. (7) we see that the obtained thermal conductivity is proportional to the ohmic heat divided by the temperature difference, *i.e.* $\lambda_{eff} \propto (I^2R)/\Delta T(x)$. The thermal conductivity will reach a steady value when the ohmic heat is so large that the temperature difference is related only to the ohmic heat. For instance, for low ohmic heat we record a too small temperature difference and thus obtain a too high value for the thermal conductivity. This can be due to the heat leakage of some kind; *e.g.* the heat is led to the side of the supercapacitor housing or ambient air. When the temperature response is too small, the effective thermal conductivity appears too large. It is only when there is so much ohmic heat that the temperature differences are solely related to the ohmic heat production that we obtain a reliable effective thermal conductivity.

The discrepancy between the obtained thermal conductivities of each experimental series is directly linked to the difference in

Table 3
Thermal conductivity, λ, determined from experimental data at cycling currents between 1.375 A and 2.0 A and electric resistance, R_{el}, measured prior to each reproduction by a high frequency ohm meter for several reproductions of three different set-ups (A, B, and C).

Experimental set-up	Thermal conductivity, λ/W K^{-1} m^{-1}			Electric resistance, R_{el}
	Series 1	Series 2	Series 3	Average $R_{A/B/C1-3}$
A	0.58 ± 0.02	0.57 ± 0.04	0.54 ± 0.04	0.529 ± 0.002
B	0.72 ± 0.03	0.70 ± 0.01	0.69 ± 0.01	0.448 ± 0.002
C	0.96 ± 0.02	0.95 ± 0.02	0.95 ± 0.02	0.475 ± 0.008

Table 4
Thermal conductivities, λ, of the material components of the supercapacitors determined *ex-situ*, at compression pressures of 4.6 bar, 9.2 bar, 13.8 bar and 16.1 bar during compression, and 4.6 bar, during decompression, listed in the respective order.

Material	Compaction pressure [bar]	Thermal conductivity, λ_i [W K^{-1} m^{-1}]
Aluminium current collectors	4.6⇑	0.633 ± 0.310
	9.2⇑	0.970 ± 0.490
	13.8⇑	1.271 ± 0.672
	16.1⇑	1.435 ± 0.777
	4.6⇓	1.223 ± 0.739
Carbon/aluminium electrodes	4.6⇑	0.641 ± 0.021
	9.2⇑	0.618 ± 0.031
	13.8⇑	0.650 ± 0.008
	16.1⇑	0.671 ± 0.019
	4.6⇓	0.663 ± 0.032
Plastic coating	4.6⇑	0.104 ± 0.020
	9.2⇑	
	13.8⇑	0.122 ± 0.012
	16.1⇑	0.125 ± 0.012
	4.6⇓	0.123 ± 0.013
Separator	4.6⇑	0.201 ± 0.011
	9.2⇑	0.215 ± 0.034
	13.8⇑	0.220 ± 0.036
	16.1⇑	0.227 ± 0.051
	4.6⇓	0.245 ± 0.085
Steel housing	4.6⇑	0.224 ± 0.102
	9.2⇑	0.195 ± 0.057
	13.8⇑	0.185 ± 0.032
	16.1⇑	0.188 ± 0.023
	4.6⇓	0.236 ± 0.028

Table 5
Average thermal conductivity of the supercapacitor component materials, λ_i, and their respective thermal resistivities relative to the total material thicknesses through the axial direction in the supercapacitor stack, r_i, obtained by method II, *ex-situ*.

Material	Thermal conductivity, λ_i [W K^{-1} m^{-1}]	Thermal resistivity, r_i [Km^2 W^{-1}]
Aluminium current collectors	1.1 ± 0.3	2.159 ± 0.694
Activated carbon/aluminium electrodes	0.649 ± 0.011	24.394 ± 0.970
Plastic coating	0.121 ± 0.008	15.861 ± 3.922
Separator	0.22 ± 0.02	10.554 ± 2.570
Steel housing	0.21 ± 0.03	28.621 ± 10.203

temperature increase as the only other factor changing in the modelling is the ohmic resistance, R. This is a little higher for the A series supercapacitor stack. Since the temperature difference between the A and the C series experiments is approximately a factor of 2, the difference in thermal conductivity is given by the same factor in accordance with Eq. (7). It is important to note that the thermal conductivity is obtained by weighing for the ohmic resistances (Table 3) and, thus, the only differences that should affect the effective thermal conductivities between each set-up is the thermal contact resistances between in each set-up. Further it is considered a strength of the model that it is able to approximate the thermal conductivity as a consistent and approximately constant value once the ohmic heat becomes substantial.

4.3. Thermal conductivity of the supercapacitor components: ex-situ measurements

In order to obtain the total thermal conductivity of the supercapacitor stack using method II, the thermal conductivities of the materials, λ_i, constituting the supercapacitor structure had to be determined *ex-situ*. The experimental method described in section 3.2 was used to obtain the thermal conductivities of the aluminium current collectors, λ_{Al}, the carbon/aluminium electrodes, λ_{el}, the plastic coating, λ_{pl}, the separator between the electrodes, λ_{sep}, and the steel housing, λ_{steel}, at different compaction pressures. From these results the thermal conductivity of the activated carbon layer of the electrodes can also be obtained.

In Table 4 the thermal conductivities of the supercapacitor materials, derived from the measurements of the thermal resistivities and sample thicknesses, are listed. The thermal conductivities were determined at compaction pressures of 4.6 bar, 9.2 bar, 13.8 bar, and 16.1 bar during compression and at 4.6 bar after decompression. The compaction pressure inside the supercapacitors is not known and the *in-situ* apparatus did not allow lighter compression than 4.6 bar to be applied to the samples. Therefore the thermal conductivities measured during compression and decompression will be averaged when applied to the model for determining the total thermal conductivity of the supercapacitor stack, λ. As seen from Table 4 the thermal conductivities of the components generally tend to increase as the compaction pressure is increased except for the thermal conductivity of the steel housing which show a decreasing trend as the compaction pressure is increased. It should be noted that the thermal conductivity of the steel samples was determined with samples that were not entirely flat due to the shape of the steel housing and the high mechanical strength of the material.

In Table 5 the average thermal conductivities of the components are presented, together with the total thermal resistivities of the respective materials, r_i. The thermal resistivities of the material components, r_i, are calculated by rearranging Eq. (13), using the averaged thermal conductivities, λ_i, the cross sectional area of

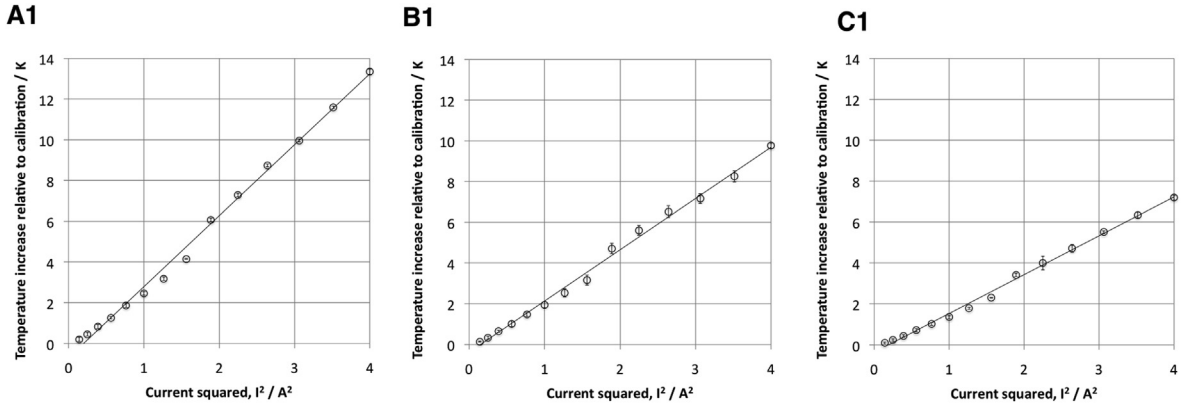

Fig. 10. Maximum temperature profile of the experiments of the A1, B1, and C1 series experiments, plotted as a function of the applied current squared I^2.

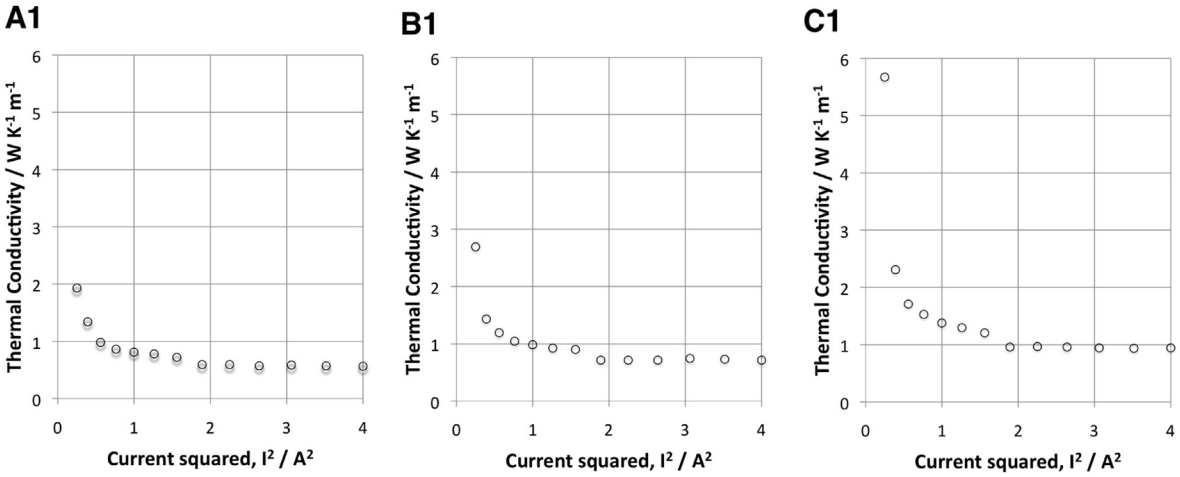

Fig. 11. Thermal conductivity, λ_{stack}, obtained by using model I on the experimental results from experiment A1, B1, and C1.

$A_{cs} = 4.5\ cm^2$, and the total thicknesses of the material components, δ_i, presented in Table 2 as parameters. Summing the component material resistivities, according to Eq. (14), the effective thermal resistivity of the supercapacitor stack is found to be $r_{stack} = 82 \pm 11\ K\ m^2\ W^{-1}$. Dividing the total thickness of all the supercapacitor stack, $\delta = 1.3 \pm 0.1$ cm, obtained from summing all the component layers in the axial direction, on the effective resistivity, r_{stack}, multiplied with the cross sectional area, A_{cs}, as described in Eq. (15), the effective thermal conductivity of the supercapacitor stack is found to be $\lambda_{stack} = 0.35 \pm 0.06\ W\ K^{-1}\ m^{-1}$. This value assumes on that the measurements of the steel casing are correct. Yet, the samples used to determined the thermal conductivity of the steel were not entirely flat and it is likely that the mechanical strength of the steel has caused air to occupy major parts of the intrinsic area between the steel samples and given rise to a thermal resistance that is not representative for the material. By using a stainless steel thermal conductivity of 15 $W\ K^{-1}\ m^{-1}$ instead of the value given in Table 5 and neglecting the standard deviation of this parameter an effective thermal conductivity of $\lambda_{stack} = 0.53 \pm 0.06\ W\ K^{-1}\ m^{-1}$ is obtained.

Using Eq. (15) reversibly for the activated carbon/aluminium electrodes, with the area of the circular samples as the area parameter, $A_{sample} = \pi(21.0 \pm 0.1\ mm/2)^2$, and assuming that the aluminium layer of the electrodes are made from the same material as the aluminium current collectors, the thermal conductivity of the activated carbon is found to be $\lambda_C = 0.19 \pm 0.10\ W\ K^{-1}\ m^{-1}$. The large uncertainty is related to the uncertainty in the thickness of the two layers as the thickness was determined as the difference in thickness before and after removing the layer mechanically with a scalpel. The average value places itself close to the value of dry the dry activated carbon supercapacitor electrode material reported by Burheim et al. [39], of $0.13 \pm 0.01\ W\ K^{-1}\ m^{-1}$. The corresponding value for the activated carbon soaked in 1 M TEA BF_4 was reported to be $0.47 \pm 0.04\ W\ K^{-1}\ m^{-1}$. 1 M TEA BF_4 was also used in the experimental procedure when determining the thermal conductivity of both the electrodes and the separator in order to recreate the conditions within the supercapacitors. The reason for the discrepancy between the two models could be due to different preparation of the activated carbon materials tested or less soaked electrodes in this experiment than in the corresponding experiment acetonitrile evaporates very quickly. In other words; drying out must be avoided in order to most appropriately supply cooling during intense cycling of supercapacitors.

4.4. Comparing the in-situ and ex-situ results

Comparing the two methods for the effective thermal conductivity, λ_{eff}, the values obtained from the *ex-situ* method, method II, is smaller than all the effective thermal conductivities obtained using the *in-situ* method, method I, in the B and C experimental series, but for the A experimental series the fit between the two models is good. Having carried out numerous dissections of the supercapacitors, it is regarded unlikely that the compaction pressure inside the supercapacitors has exceeded the compaction pressures applied in the determination of the component material thermal conductivities, λ_i, in method II. This implies that the capacitor unit internal compaction pressure cannot be the reason for the misfit between the two methods, as the thermal conductivity generally is expected to increase with increasing compaction pressure. On the other hand, the discrepancy of the thermal conductivities from method I is assumed to be due to the contact between each capacitor unit in the calorimeter. The two methods do, therefore, show common effective thermal conductivities when the inter-capacitor-unit contact appears the highest, *i.e.* set-up A.

There are three other possible reasons for the discrepancy between the two methods; namely that the encapsulation of the supercapacitors can give a major contribution to the thermal conductivity of the supercapacitor stack estimated in method I, that the effective thermal conductivity varies from the centre to the edge or that the thermal paste between the supercapacitors in the calorimetric experiments has given rise to a higher thermal conductivity than what has been taken account for in method II. A high conductance of the thermal paste that is neglected in method II would give a positive contribution to the thermal conductivity in method I that has not been taken account for in method II. This may also be due to the plastic coating and contact resistance between this plastic and the steel housing. Hence, there is good reason to assume that the real value of the effective supercapacitor stack thermal conductivity, λ_{stack}, can be expected to be somewhere in between the values obtained from method I and II, *i.e.* $0.5–1.0\ W\ K^{-1}\ m^{-1}$.

Studying the thermal resistivities displayed in Table 4, and assuming that the thermal conductivity of the steel casing is closer to 15 $W\ K^{-1}\ m^{-1}$ than the 'uncertain' values obtained from the experiments, it is evident that it is the activated carbon/aluminium electrodes reside the highest thermal resistivity of the constituent material layers. Assuming that the aluminium of the electrodes is the same material as used in the current collectors; the main

contribution to the thermal resistivity of the electrodes is the activated carbon layer. This indicates that the activated carbon electrode material is the most important contributor to internal temperature gradients in supercapacitor units. Therefore, this is also the most important material to focus on when engineering heat in relation to supercapacitors. Additionally, the obtained values compared well to our previous study [39] and demonstrates the importances of the published series on studies of thermal conductivity measurements.

5. Conclusion

- Embedding thermocouples between four stacked commercial supercapacitors, analysed in the light of the first law of thermodynamics, an effective thermal conductivity, λ_{eff}, between 0.5 W K^{-1} m^{-1} and 1.0 W K^{-1} m^{-1}, is obtained.
- Measuring the thermal conductivity of each component independently an effective thermal conductivity of $\lambda_{eff} = 0.53 \pm 0.06$ W K^{-1} m^{-1}, is obtained.
- When evaluating stacks of supercapacitors, the contact between the single supercapacitors appears the most important factor for the overall heat management. When evaluating the effective thermal conductivity of each single supercapacitor, the thermal conductivity of the active electrode is the most important factor.

Acknowledgement

The INM is part if the Leibniz Research Alliance Energy Transition (LVE). Volker Presser acknowledges financial support from the German Federal Ministry for Research and Education (BMBF) in support of the nanoEES3D project (award number 03EK3013) as part of the strategic funding initiative energy storage framework. Volker Presser thanks Professor Arzt for his continuing support.

HiST is acknowledged for funding open access of this paper.

References

[1] Béguin F, Presser V, Balducci A, Frackowiak E. Carbons and electrolytes for advanced supercapacitors. Adv Mater 2014;26(14):1521–4095.
[2] Simon P, Gogotsi Y. Materials for electrochemical capacitors. Nat Mater 2008;7:845–54.
[3] Miller JR. Valuing reversible energy storage. Science 2012;335:1312–3.
[4] Musolino V, Pievatolo A, Tironi E. A statistical approach to electrical storage sizing with application to the recovery of braking energy. Energy 2011;36:6697–704.
[5] Huang T-C, Leu Y-G, Chang Y-C, Hou S-Y, Li C-C. An energy harvester using self-powered feed forward converter charging approach. Energy 2013;55:769–77.
[6] Kühne K. Electric buses – an energy efficient urban transportation means. Energy 2010;35:4510–3.
[7] http://www.spectrum.ieee.org/green-tech/advanced-cars/the-charge-of-the-ultra capacitors.The charge of the ultra – capacitors: nanotechnology takes energy storage beyond batteries. 2007 [Retrieved January 8th 2014].
[8] http://www.maxwell.com/ultracapacitors/. Maxwell ultracapacitors: enabling energy's future. [Retrieved January 8th 2014].
[9] Dargahi V, Sadigh AK, Pahlavani MRA, Shoulaie A. DC (direct current) voltage source reduction in stacked multicell converter based energy systems. Energy 2012;46(1):649–63.
[10] Rodrigues EMG, Godina R, Santos SF, Bizuayehu AW, Contreras J, Catalão JPS. Energy storage systems supporting increased penetration of renewables in islanded systems. Energy 2014;75:265–80.
[11] Kamel RM, Chaouachi A, Nagasaka K. Wind power smoothing using fuzzy logic pitch controller and energy capacitor system for improvement microgrid performance in islanding mode. Energy 2010;35:2119–29.
[12] Christen T, Carlen MW. Theory of the ragone plots. J Power Sources 2000;91:210–6.
[13] Pell WG, Conway BE. Quantitative modeling of factors determining ragone plots for batteries and electrochemical capacitors. J Power Sources 1996;63(2):255–66.
[14] Conway BE. Transition from “supercapacitor” to “battery” behavior in electrochemical energy storage. J Electrochem Soc 1991;138:1539–48.
[15] Pandolfo AG, Hollenkamp AF. Carbon properties and their role in supercapacitors. J Power Sources 2006;157:11–27.
[16] Miller JR, Simon P. Fundamentals of electrochemical capacitor design and operation. Electrochem Soc Interface 2008;17:31–2.
[17] Lin Rongying, Taberna Pierre-Louis, Fantini Sébastien, Presser Volker, Pérez Carlos R, Malbosc François, et al. Capacitive energy storage from -50 to 100 c using an ionic liquid electrolyte. J Phys Chem Lett 2011;2(19):2396–401.
[18] Frackowiak E, Béguin F. Carbon materials for the electrochemical storage of energy in capacitors. Carbon 2001;39:937–50.
[19] Burke A. Ultracapacitors: why, how, and where is the technology. J Power Sources 2000;91:37–50.
[20] Zhang LL, Zhao XS. Carbon-based materials as supercapacitor electrodes. Chem Soc Rev 2009;38:2520–31.
[21] Inagaki M, Konno H, Tanaike O. Carbon materials for electrochemical capacitors. J Power Sources 2010;195:7880–903.
[22] Béguin F, Frackowiak E. Carbons for electrochemical energy storage and conversion systems. Boca Raton: CRC Press; 2009.
[23] Stoller MD, Ruoff RS. Best practice methods for determining an electrode material's performance for ultracapacitors. Energy Environ Sci 2010;3:1294–301.
[24] Burke A, Miller M. Testing of electrochemical capacitors: capacitance, resistance, energy density, and power capability. Electrochim Acta 2010;55:7538–48.
[25] Gogotsi Y, Simon P. True performance metrics in electrochemical energy storage. Science 2011;334:917–8.
[26] Azais P, Duclaux L, Florian P, Massiot D, Lillo-Rodenas M-A, Linares-Solano A, et al. Causes of supercapacitors ageing in organic electrolyte. J Power Sources 2007;171:1046–53.
[27] Ruch PW, Cericola D, Foelske-Schmitz A, Kötz R, Wokaun A. Aging of electrochemical double layer capacitors with acetonitrile-based electrolyte at elevated voltages. Electrochim Acta 2010;55:4412–20.
[28] Miller JR, Burke AF. Electrochemical capacitors: challenges and opportunities for real-world applications. Electrochem Soc Interface 2008;17:53–7.
[29] Virtanen A, Haapala H, Hannikainen S, Muhonen T, Tuusa H. Calorimetric efficiency measurements of supercapacitors and lithium-ion batteries. In: Conference proceedings – IEEE applied power electronics conference and exposition – APEC; 2011. p. 1367–73.
[30] Gualous H, Louahlia H, Gallay R. Supercapacitor characterization and thermal modelling with reversible and irreversible heat effect. IEEE Trans Power Electron 2011;26:3402–9.
[31] d'Entremont A, Pilon L. First-principles thermal modeling of electric double layer capacitors under constant-current cycling. J Power Sources 2014;246:887–98.
[32] Lin R, Divay L, Le Barney P, Pham Thi M, Taberna P-L, Simon P, et al. Self-standing electrochemical double layer capacitors for operation in severe temparature conditions. Mater Renew Sustain Energy 2013:1–7.
[33] Wang Kai, Zhang Li, Ji Bingcheng, Yuan Jinlei. The thermal analysis on the stackable supercapacitor. Energy 2013;59:440–4.
[34] Gualous H, Bouquain D, Berthon A, Kauffmann JM. Experimental study of supercapacitor serial resistance and capacitance variations with temperature. J Power Sources 2003;123(1):86–93.
[35] Klemens PG, Pedraza DF. Thermal conductivity of graphite in the basal plane. Carbon 1994;32:735–41.
[36] Balandin AA, Ghosh S, Bao W, Calizo I, Teweldebrhan D, Miao F, et al. Superior thermal conductivity of single-layer graphene. Nano Lett 2008;8:902–7.
[37] Che J, Çağin T, Goddard III WA. Thermal conductivity of carbon nanotubes. Nanotechnology 2000;11:65–9.
[38] Cacciola G, Restuccia G, Mercadante L. Composites of activated carbon for refrigeration adsorption machines. Carbon 1995;33:1205–10.
[39] Burheim OS, Aslan M, Atchinson JS, Presser V. Thermal conductivity and temperature profiles in carbon electrodes for supercapacitors. J Power Sources 2014;246:160–6.
[40] Bird RB, Stewart WE, Lightfoot EN. Transport phenomena. 2nd ed. John Wiley and Sons; 2007.
[41] Burheim OS, Onsrud MA, Pharoah JG, Vullum-Bruer F, Vie PJS. Thermal conductivity, heat sources and temperature profiles of li-ion batteries. ECS Trans 2014;58:145–71.
[42] Burheim OS, Su H, Hauge HH, Pasupathi S, Pollet B. Study of thermal conductivity of pem fuel cells catalyst layers. Int J Hydrogen Energy 2014;39:9397–408.
[43] Burheim OS, Su H, Pasuphati S, Pharoah JG, Pollet BG. Thermal conductivity and temperature profiles of the micro porous layers used for the polymer electrolyte membrane fuel cell. Int J Hydrogen Energy 2013;38:8437–47.
[44] Burheim O, Vie PJS, Møller-Holst S, Pharoah JG, Kjelstrup S. A calorimetric analysis of a polymer electrolyte fuel cell and the production of H_2O_2 at the cathode. Electrochim Acta 2010;5:935–42.
[45] http://www.maxwell.com/products/ultracapacitors/products/pc10 series.Downloads: product guide. May 25 2014. p. 1–54.
[46] Burheim O, Kjelstrup S, Pharoah JG, Vie PJS, Møller-Holst S. Calculation of reversible electrode heats in the proton exchange membrane fuel cell from calorimetric measurements. Electrochim Acta 2011;5:935–42.